z axes were used. An average image was calculated from the DWI as the mean intensity of the three images. The ADC was estimated as the mean diffusivity in the three orthogonal directions.

The dynamic susceptibility contrast-enhanced perfusion-weighted MRI (PWI) studies were performed with a single-shot, gradient-echo, echo planar pulse sequence (TE, 66milliseconds; TR, 1 second; flip angle, 90 degrees; field of view, 23cm; slice thickness, 5mm) after a bolus injection of 0.1mmol/kg body weight of the paramagnetic contrast medium gadolinium-diethylenetriaminepentaacetic acid (Gd-DTPA, Magnevist; Schering, Berlin, Germany) into the antecubital vein through an 18-gauge catheter with the use of an automatic injector. With 60 time points over the 4 slices at 0, 12, 24, and 36mm above and parallel to the AC-PC line, we created a quantitative image of the mean transit time (MTT) on MR Vision software (MR Company, Seimens, Erlangen, Germany) using the method of Schreiber and colleagues.[16] This method is based on the principles of the indicator dilution theory and processing the signal time curves with deconvolution analysis. One slice including the MCA of the unaffected hemisphere was selected to measure the arterial input function (AIP). Regional CBV (rCBV) values were calculated by:

$$rCBV = \frac{KH}{\rho} \cdot \frac{\int_0^\infty C_m(t)dt}{\int_0^\infty AIP(t)dt} \quad (1)$$

where ρ is the density of brain tissue ($\rho = 1.04gm/mm^3$), and $C_m(t)$ is the measured concentration time curve on a pixel-by-pixel basis using the well-established relation for purely susceptibility weighted MR sequences. K_H is the correction factor that takes into account the different hematocrit in capillaries and the large arterial vessels. To eliminate tracer recirculation, we performed integration of $C_m(t)$ in Equation 1 from the start of the bolus to the measurement where $C_m(t)$ had decreased to 30% of the peak bolus concentration in that pixel. The MTT values were obtained from the area-over-height relation by:

$$MTT = \frac{\int_0^\infty R(t)dt}{R(t=0)} \quad (2)$$

where R(t) is the residue; that is, the amount of tracer remaining in the voxel at time t since bolus arrival. Because an infinitely short bolus input into a voxel cannot be achieved in an in vivo study, the measured concentration time curve in the brain parenchyma, $C_m(t)$, is related to the residue by:

$$C_m(t) = KH^{-1}AIP \otimes R(t) \quad (3)$$

where $\otimes$ denotes the convolution operation. MTT was calculated by orthogonal polynomial deconvolution of Equation 3.

Because a previous study has demonstrated that the degree of expansion of the initial DWI lesion proportionally correlates with MTT prolongation and the volume of MTT greater than 4 or greater than 6 seconds was the most predictable for the final infarct size compared with the CBV or CBF,[17] we used an MTT image as a representative of the PWI to detect areas with impaired cerebral circulation. The average window level of the MTT image was 6 seconds for image demonstration for the determination of areas with any perfusion abnormality.

Positron Emission Tomography

In eight patients, the PET study was done immediately after the MRI study. In the other three patients (Patients 5, 6, and 9), the PET study was followed by the MRI study. The PET measurements were performed with a Headtome V (Shimadzu, Kyoto, Japan) after patients inhaled a trace amount of $^{15}O_2$ and received an intravenous injection of $H_2{}^{15}O$. Based on these measurements, we have developed a method for estimating relCBF, relCMRO$_2$, and relOEF without arterial blood sampling. Regional CBF, OEF, and CMRO$_2$ were determined as relative to values of the corresponding brain structures in the contralateral hemisphere by means of a calibration curve procedure. The calibration curve related the relCBF to the relative $H_2{}^{15}O$ count, the relCMRO$_2$ to the relative $^{15}O_2$ count, and the relOEF to the relative $^{15}O_2/H_2{}^{15}O$ count. The theory and the error analysis were described previously elsewhere.[18] Briefly, in six patients with chronic unilateral occlusion of the internal carotid artery or MCA, the CBF, CMRO$_2$, OEF, and CBV were estimated quantitatively. For region of interest (ROI) analysis to calculate the lesion/contralateral hemisphere ratio of the CBF, OEF, CMRO$_2$, $H_2{}^{15}O$, $^{15}O_2/H_2{}^{15}O$, and $^{15}O_2$, circular ROIs 16mm in diameter covered the cerebral cortex at the slice level of 0, 12, 24, and 36mm above and parallel to the AC-PC line. The relative $H_2{}^{15}O$ count was plotted against the relCBF. The $^{15}O_2$ image was corrected for intravascular $^{15}O_2$ by assuming the mean CBV to be 4ml/100gm. The relative $^{15}O_2$ count then was plotted against the relCMRO$_2$. The relative $^{15}O_2/H_2{}^{15}O$ count was plotted against the relOEF. By the least square-fitting method, the calibration curves were obtained for the relative $H_2{}^{15}O$, relative $^{15}O_2$, and relative $^{15}O_2/H_2{}^{15}O$. By means of these calibration curves, relative $H_2{}^{15}O$, relative $^{15}O_2$, and relative $^{15}O_2/H_2{}^{15}O$ counts as measured in our patients were converted to relCBF, relCMRO$_2$, and relOEF values.

Data Analysis

All the DWI, ADC, PWI, $H_2{}^{15}O$, and $^{15}O_2$ images were transferred to a Unix workstation (TITAN 750; Kubota Computers, Tokyo, Japan). Because turbo spin-echo T2-weighted imaging has a smaller degree of peripheral distortion caused by susceptibility artifacts than echo planer DWI, we registered the $H_2{}^{15}O$ images to the T2-weighted imaging at day 3 using the automatic multimodality image registration software developed by Ardekani and colleagues.[19] We first segmented the MR image into a number of spatially contiguous components using K-means clustering and connected components analysis. Six rigid body pa-

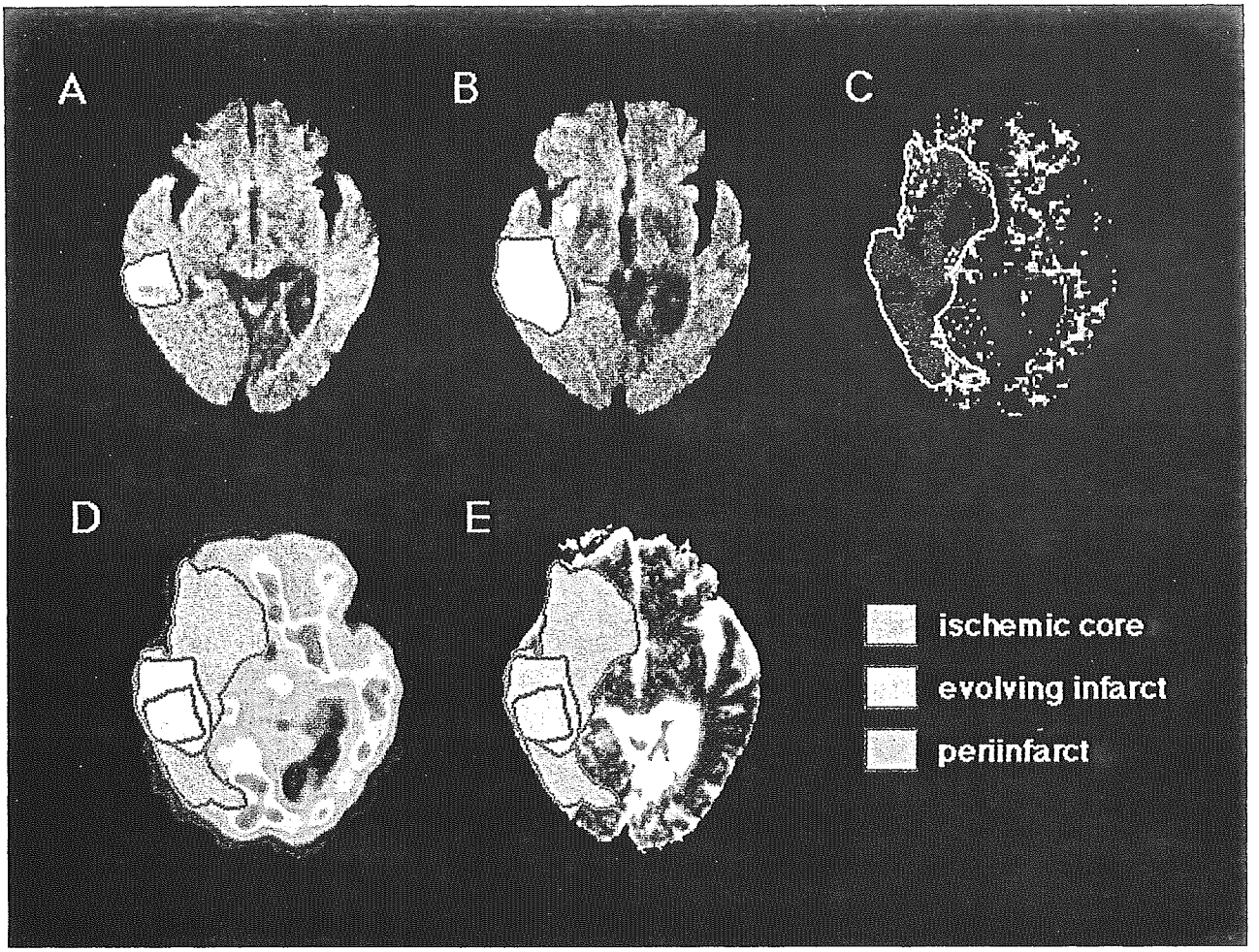

Fig 1. Application of regions of interest (ROIs) on ischemic core, evolving infarct, and perrinfarct. All PET and ADC images are registered to T_2WI obtained at day 3, and the corresponding four slice levels to PWI is selected for analysis. The ROIs of ischemic core, periinfarct, and evolving infarct are manually drawn on (A) the initial DWI within 6 hours after onset, (B) DWI performed at day 3, and (C) PWI obtained at the time of initial DWI. The ROIs are automatically superimposed on the corresponding (D) PET and (E) ADC images and are mirrored to the contralateral unaffected hemisphere.

rameters (three translations and three rotations) then were found such that when the $H_2{}^{15}O$ images were matched to the T2-weighted images with these parameters, the total sum of squared deviations from the mean $H_2{}^{15}O$ image within all connected components was minimized. These parameters were applied to the $^{15}O_2$ images. Because the T2-weighted imaging at day 3 and initial DWI on admission were based on the same AC-PC line determined by a midsagittal T1-weighted image, the initial DWI, ADC, $H_2{}^{15}O$, and $^{15}O_2$ images and the T2-weighted imaging and DWI at day 3 were all in registration. The $^{15}O_2/H_2{}^{15}O$ image was created by dividing the registered $^{15}O_2$ image by the registered $H_2{}^{15}O$ image. The PWIs were obtained at 0, 12, 24, and 36mm above and parallel to the AC-PC line. Therefore, the PWIs also were registered in these slice levels to the T2-weighted images. The four planes corresponding to the PWI images were used for analysis of the registered PET and the ADC images.

Determination of the Ischemic Core, Evolving Infarct, and Periinfarct

Because the perfusion imaging was performed at 0, 12, 24, and 36mm above and parallel to the AC-PC line, the volume of the ischemic core, evolving infarct, and periinfarct was measured within these four slices. We defined three distinct lesions in the affected vascular territory based on the initial and follow-up MR studies; the ischemic core represented by abnormal diffusion on the initial DWI; the evolving infarct defined as normal diffusion at the initial DWI, but abnormal at the follow-up DWI on day 3; and the periinfarct defined as normal diffusion through the initial and follow-up DWI within abnormal perfusion on the initial PWI. The ROIs for the ischemic core, evolving infarct, and periinfarct were drawn manually on the initial and follow-up MR images (Fig 1). Each ROI was copied to the registered $H_2{}^{15}O$, $^{15}O_2$, $^{15}O_2/H_2{}^{15}O$, and ADC image and was automatically mirrored to the contralateral unaffected hemisphere.

Statistical Analysis

Because we could not prove the normality of these data probably because of the limited sample size, nonparametric statistics were used. Multiple comparisons of the PET and ADC ROI data among the three lesion types were performed with the Kruskal–Wallis test and Steel–Dwass procedure. $p < 0.05$ was considered statistically significant. The Wilcoxon signed rank test was used for analysis of the relCBF, relCMRO$_2$, and relOEF for comparison with unity. A discriminant analysis was performed to determine the best cutoff function between the ischemic core and the evolving infarct and between the evolving infarct and the periinfarct under the normality assumption.

Results

Volume of the Ischemic Core, Evolving Infarct, and Periinfarct

Table 2 shows the volume of the ischemic core, evolving infarct, and periinfarct in each patient. The volume was a sum of four tomographical slices where the PWI and DWI were performed. The volume of the ischemic core was less than 5ml in five patients. The volume of the evolving infarct was less than 5ml in four patients. These lesions were excluded from this analysis because inaccuracy caused by partial volume averaging was anticipated. The periinfarct lesion was found in 9 of 11 patients. In the other two patients, the extent of the diffusion abnormality was identical to that of the perfusion abnormality. The volume of the ischemic core and evolving infarct for the entire lesion (a sum of 19 tomographical slices where the DWI was performed) also is shown in parentheses in Table 2.

Table 2. Volume of Ischemic Core, Evolving Infarct, and Periinfarct on Registered MRI

Patient No.	Ischemic Core (ml)	Evolving infarct (ml)	Periinfarct (ml)
1	− (6.3)	20.5 (63.7)	23.8
2	83.7 (187.9)	28.1 (56.2)	10.4
3	12.6 (47.4)	11.9 (40.6)	10.9
4	8.2 (11.4)	17.6 (48.4)	20.4
5	21.7 (18.8)	81.7 (255.5)	21.4
6	63.8 (127.4)	38.5 (119.8)	7.1
7	− (6.3)	− (0)	35.2
8	− (8.0)	− (8.1)	18.6
9	− (4.5)	− (2.1)	28.9
10	56.1 (109.0)	69.2 (192.6)	-
11	− (4.6)	− (0)	-
Mean ± 1SD	41.0 ± 31.1	38.2 ± 27.0	19.6 ± 9.1

The volume of each lesion was a sum of four registered tomographic slices in which MR perfusion imaging and diffusion imaging were performed. In parentheses, the volume of the ischemic core and evolving infarct for the entire lesion (a sum of 19 registered tomographic slices where MR diffusion imaging was performed initially and on day 3) is shown.
MRI = magnetic resonance imaging; SD = standard deviation.

Relative Cerebral Blood Flow, Relative Oxygen Extraction Fraction, and Relative Cerebral Metabolic Rate of Oxygen

The calibration curves relating the relative $H_2{}^{15}O$, $^{15}O_2$, $^{15}O_2/H_2{}^{15}O$ counts to the relCBF, relCMRO$_2$, and relOEF, respectively, are shown in Figure 2. The calibration curve between the relCBF (x) and the relative $H_2{}^{15}O$ counts (y) was $y = 0.11x^3 - 0.55x^2 + 1.41x + 0.03$ ($r = 0.99$; $p < 0.001$; n = 115). The calibration curve between the relCMRO$_2$ (x) and the relative $^{15}O_2$ (y) was $y = -0.26x^3 + 0.36x^2 + 0.77x + 0.18$ ($r = 0.94$; $p < 0.001$; n = 115). The calibration curve between the relOEF (x) and the relative $^{15}O_2/H_2{}^{15}O$ (y) was $y = 7.62x^3 - 0.16x^2 + 0.86x + 0.25$ ($r = 0.95$; $p < 0.001$; n = 115).

Table 3 summarizes the mean relCBF, relCMRO$_2$, and relOEF for the ischemic core, evolving infarct, and periinfarct lesions. The mean relCBF and relCMRO$_2$ for the three lesion types showed a significant reduction compared with unity ($p < 0.05$ for the ischemic core and evolving infarct; $p < 0.01$ for the periinfarct). The mean relOEF for the evolving infarct and the periinfarct showed a significant increase compared with unity ($p < 0.05$ for the evolving infarct; $p < 0.01$ for the periinfarct), but that for the ischemic core did not. The mean relCBF and mean relCMRO$_2$ for the evolving infarct were significantly greater than those for the ischemic core ($p < 0.05$ and $p < 0.05$, respectively), and significantly less than those for the periinfarct ($p < 0.05$ and $p < 0.01$, respectively). The mean relOEF for the evolving infarct did not differ significantly from that for the periinfarct.

Figure 3 is a scatterplot of the relCBF, relOEF, and relCMRO$_2$ for the ischemic core, the evolving infarct, and the periinfarct lesions. The best cutoff value to discriminate between the evolving infarct and the periinfarct was 0.49 for relCBF ($p < 0.0001$) and 0.62 for relCMRO$_2$ ($p < 0.0001$). The best cutoff value to discriminate between the ischemic core and the evolving infarct was 0.35 for relCBF ($p < 0.006$) and 0.45 for relCMRO$_2$ ($p < 0.005$).

Figure 4 shows PWIs and DWIs 80 minutes after onset; DWIs at day 3; and PET $H_2{}^{15}O$, $^{15}O_2$, and $^{15}O_2/H_2{}^{15}O$ images obtained 110 minutes after onset in Patient 4. The area of the DWI lesion was remarkably enlarged on the DWI at day 3 compared with the initial DWI lesion. A moderate reduction in the relCMRO$_2$ is evident in the area of volume expansion of infarction.

Apparent Diffusion Coefficient for the Ischemic Core, Evolving Infarct, and Periinfarct

The lesion-to-contralateral ratio of the quantitative ADC was defined as relative ADC (relADC). The mean relADC value for the ischemic core, evolving in-

farct, and periinfarct was 0.66 ± 0.05, 0.93 ± 0.09, and 0.95 ± 0.09, respectively. The mean relADC for the ischemic core was significantly less than that for the periinfarct and the evolving infarct ($p < 0.01$). There was no significant difference in relADC between the periinfarct and the evolving infarct.

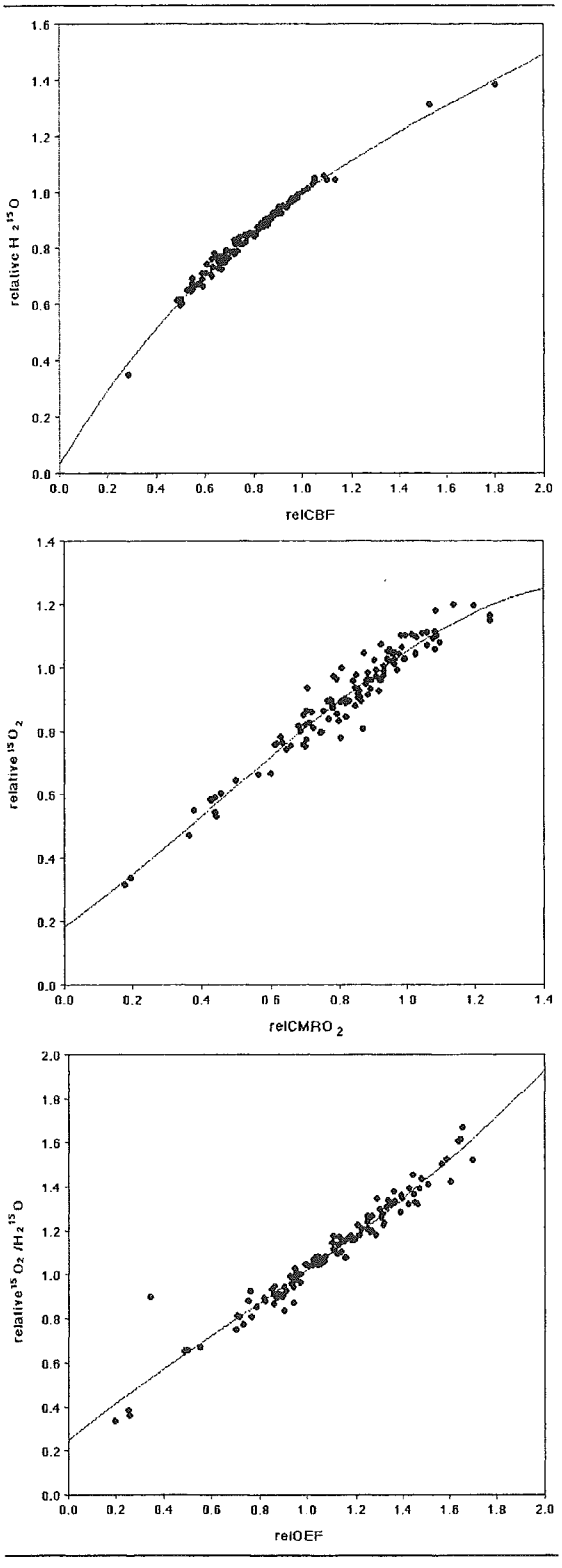

Fig 2. Calibration curves relating relative PET counts to relative quantitative PET values in patients with chronic stenoocclusive disease of carotid or cerebral artery in another series of the PET study. Polynominal curve fitting with order 3 demonstrated a good relationship between (A) relCBF versus relative $H_2{}^{15}O$ ($y = 0.11x^3 - 0.55x^2 + 1.41x + 0.03$, $r = 0.99$, $p < 0.001$, $n = 115$), (B) relCMRO$_2$ versus relative $^{15}O_2$ ($y = -0.26x^3 + 0.36x^2 + 0.77x + 0.18$, $r = 0.94$, $p < 0.001$, $n = 115$), and (C) relOEF versus relative $^{15}O_2/H_2{}^{15}O$ ($y = 7.62x^3 - 0.16x^2 + 0.86x + 0.25$, $r = 0.95$, $p < 0.001$, $n = 115$), respectively.

Discussion

This prospective study demonstrated that the volume expansion of acute embolic infarction during the first 3 days was preceded by a reduction in the cerebral oxygen metabolism as early as 6 hours after onset but was not associated with reduction of the ADC of water. Within the perfusion–diffusion mismatch, a relCMRO$_2$ less than 0.62 was indicative of evolution into an infarction.

The volume expansion of a brain infarction based on the CT hypodensity was correlated with the CBF, OEF, and CMRO$_2$ in stroke patients.[20,21] Furlan and colleagues[21] define the ischemic core (area 3 in their study) as a hypodense lesion on initial CT examination; they define the infarcted penumbra (area 1) as a normodense lesion on initial CT with high OEF and a CBF range from 10 to 20ml/100gm/min; they define the noninfarcted penumbra (area 2) as a normodense lesion on initial CT with high OEF and a CBF range from 10 to 20ml/100gm/min; and they define oligemia as a normodense lesion on initial CT with high OEF and a CBF range of more than 20ml/100gm/min (area 4). They indicate that the infarcted penumbra, which corresponded to the evolving infarct of our study, showed 0.55 in relCMRO$_2$. This value, which was determined 7 to 18 hours after onset, was fairly consistent with this study's value for the evolving infarct (0.53). The results obtained by the CT-based study and this MRI-based study indicated that the cerebral oxygen metabolism of the evolving infarct decreased to about 50% of the reference level within 6 hours of onset and continued to be low during 18 hours. The relative cerebral oxygen metabolism in the evolving infarct was significantly greater than that of the DWI lesion in this study and the previously infarcted lesion in the CT-based study (0.53 vs 0.30 in this study; 0.55 vs 0.37 in the work by Furlan and colleagues[21]).

In their experimental study, Giffard and colleagues[22] demonstrate with a 20-hour occlusion and reperfusion model in the baboon that the evolving infarct showed CBF reduction similar to the ischemic core 1 hour after occlusion and continued for 20 hours. The relCMRO$_2$ of the evolving infarct 1 hour

after occlusion (0.68) gradually decreased to the same level of the previously infarcted lesion during 20 hours of occlusion (0.44). In stroke patients, Marchal and colleagues[23] report that cerebral oxygen metabolism in later infarcted lesions was relatively maintained within 7 to 16 hours of onset (≤4.13ml/100gm/min) and was associated with increased OEF but eventually decreased to the level of the evolving infarction (<1.40ml/100gm/min) at the chronic stage. Heiss and colleagues[24] report that the $CMRO_2$ in the borderzone of ischemia with increased OEF deteriorated during the 13- to 25-day observation period. These previous CT-based studies indicate that, in some ischemic brain tissue, the $CMRO_2$ gradually decreases in some portions.

The reduction of the $CMRO_2$ in the evolving infarct was not associated with a reduction in the ADC within 6 hours of onset. The ADC change was related to cellular energy failure and early cytotoxic edema.[25–29] Sakoh and colleagues[30] investigated the ADC for the evolving infarct in the MCA occlusion pig model. In their study, all areas with an ADC less than 75% of the reference area progressed to infarction after 2 hours of MCA occlusion. In the recent acute human stroke studies, the relADC in the evolving infarct was not significantly reduced in one study,[31] and it was significantly reduced but only slightly in the other.[32] In this study, no significant difference in the relADC between the evolving infarct and periinfarct was found. These results may imply that adenosine triphosphate synthesis is still preserved to a degree sufficient to maintain an adenosine triphosphate–dependent neuronal membrane ion pump in the area of the evolving infarct as early as 6 hours after onset.

Can the evolving infarct be prevented by early reperfusion? Baron and colleagues[33] demonstrate that brain infarction was prevented by early restoration of the CBF in patients with a unilateral internal carotid artery occlusion accompanied by repeated transient ischemic attacks. Young and colleagues[34] report that reperfusion after 6 hours of unilateral MCA occlusion reduced the infarct volume compared with permanent occlusion in the anesthetized baboon. They also investigated the CBF, OEF, and $CMRO_2$ in the 6-hour unilateral

Table 3. Mean Relative PET Values

	Ischemic Core	Evolving Infarct	Periinfarct
relCBF	$0.24 \pm 0.11^{a,c}$	$0.42 \pm 0.07^{b,e}$	$0.57 \pm 0.10^{b,f}$
$relCMRO_2$	$0.30 \pm 0.13^{c,e}$	$0.53 \pm 0.07^{c,d,e}$	$0.76 \pm 0.10^{d,f}$
relOEF	1.18 ± 0.22	1.31 ± 0.15^{e}	1.38 ± 0.17^{f}

$^{a}p < 0.05$; $^{b}p < 0.05$; $^{c}p < 0.05$; $^{d}p < 0.01$; $^{e}p < 0.05$; $^{f}p < 0.01$; and compared with unity.

PET = positron emission tomography.

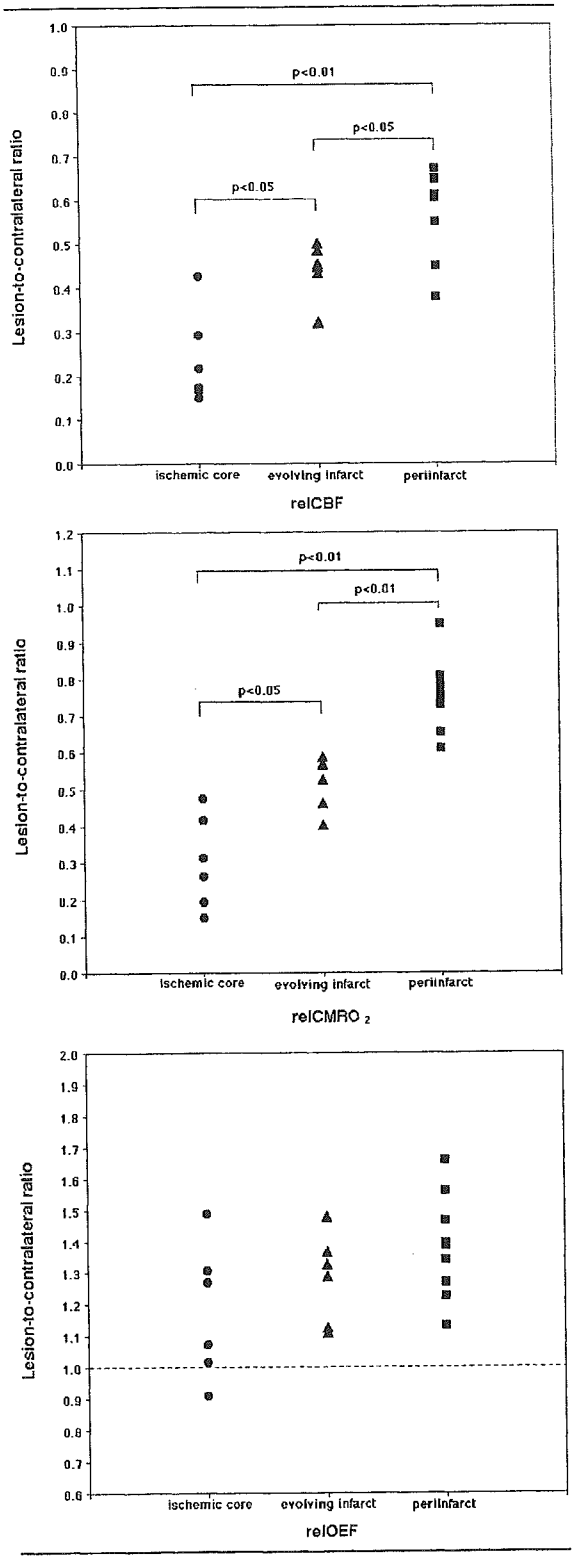

Fig 3. Scatter plots of (A) relCBF, (B) $relCMRO_2$ and (C) relOEF for ischemic core, evolving infarct, and periinfarct. The best cutoff value between evolving infarct and periinfarct was 0.49 for relCBF ($p < 0.0001$) and 0.62 for $relCMRO_2$ ($p < 0.0001$). The best cutoff value between evolving infarct and ischemic core was 0.35 for relCBF ($p < 0.006$) and 0.45 for $relCMRO_2$ ($p < 0.005$).

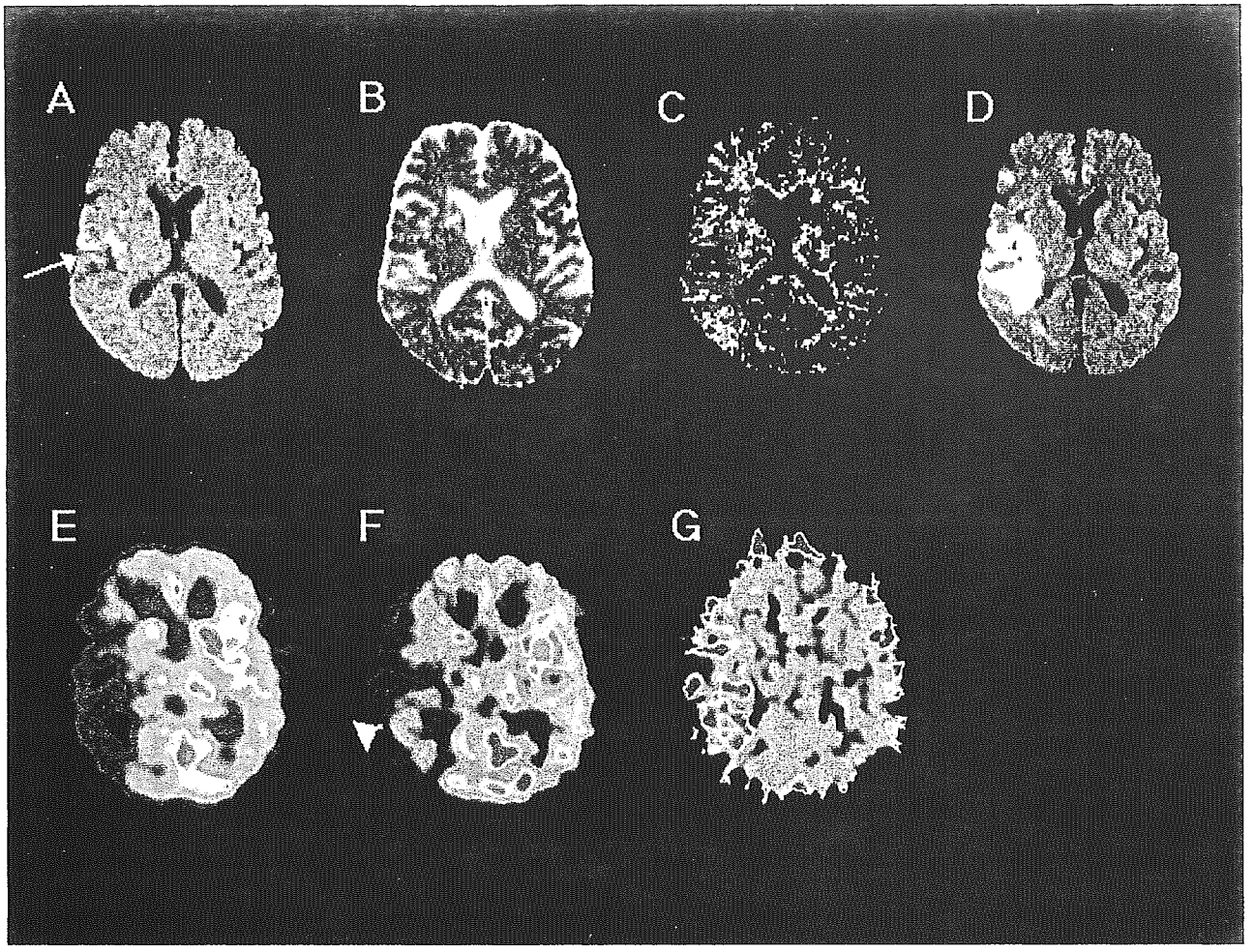

Fig 4. A 65-year-old woman with sudden onset of left hemiparesis and loss of consciousness. Cerebral angiography on admission revealed complete occlusion of right middle cerebral artery. (A) The initial DWI, (B) ADC image, (C) PWI obtained 80 minutes after onset demonstrated a small area with DWI abnormality (white arrow) and large perfusion-diffusion mismatch in right temporal lobe. (D) Follow-up DWI performed at day 3 showed enlargement of the DWI lesion, which was smaller than perfusion abnormality on initial PWI. PET images were performed 110 minutes after onset, and corresponding (E) relCBF image, (F) relCMRO$_2$ image, (G) relOEF image to initial MRI demonstrated moderate reduction of relCMRO$_2$ in the area of lesion volume expansion (white arrowhead), where diffusivity of water molecule was preserved on ADC image.

MCA occlusion and reperfusion anesthetized baboon model.[35] Reperfusion after 6 hours of occlusion prevented the infarction when the $CMRO_2$ was 0.89 at 4 hours of occlusion but not when the $CMRO_2$ was 0.59. These findings indicate that the evolving infarct could be potentially prevented by early reperfusion when the $CMRO_2$ is maintained above a certain threshold for infarction. This view is supported by a report that the use of recombinant tissue plasminogen activator resulted in a greater recanalization rate and less expansion of the DWI lesion in acute ischemic stroke.[36] The "metabolic penumbra" defined as normal water diffusion associated with the relCMRO$_2$ ranging from 0.45 (discriminating value between the ischemic core and evolving infarct) to 0.62 (discriminating value between the evolving infarct and periinfarct) is a critical target to reduce the volume expansion of brain infarction.

Although examination with a count-based PET is feasible during an emergency situation, there are several methodological limitations.[14,15,18] First, the relCBF, relCMRO$_2$, and relOEF values derived from a count-based PET are less accurate than those based on the absolute quantification because of the nonlinear correlation between radioactivity and physiological parameters. Our preliminary analysis indicated a good correlation between the count ratio and the CBF ratio by correcting for $H_2{}^{15}O$ leaving the brain. However, the relCBF calibration curve was determined by a few points at its upper and lower extremes. Second, we assumed the CBV to be uniform in the whole brain (4ml/100ml). Furlan and colleagues[21] report that the

mean CBV for normal gray matter, infarcted penumbra, and noninfarcted penumbra was 3.80, 3.40, and 3.07, respectively. Accordingly, the CBV difference between normal gray matter, the evolving infarct, and the periinfarct may be a source of error. The underestimation or overestimation of the relCMRO$_2$ in a count-based PET is less than 2% when the actual CBV difference is within 1%.[18] Third, patients with severe neurological symptoms were included. Loss of consciousness with hemispheric stroke might imply bilateral damage. The use of contralateral hemisphere for relative measurement of CBF thus might be a source of inaccuracy when the lesion-to-contralateral ratio is applied in the evaluation. Fourth, the limited spatial resolution of the PET scanner is a potential source of errors when a small structure is analyzed. In this study, we selected a lesion volume larger than 5ml to avoid this effect. Fifth, the different magnitude of partial volume averaging and the different slice thicknesses between perfusion and diffusion MRI and PET might inherently limit the accuracy even after the image coregistration. Sixth, only five perfusion images, not the entire brain, were analyzed because of the limited capability of perfusion MRI. Finally, the application of the discriminant analysis relies on the normality of the data. Under this assumption, we used the discriminant analysis to determine the best cutoff values of relCBF and relCMRO$_2$ between the lesion types. However, the normality of our data remained uncertain.

In conclusion, despite the methodological problems and the limited number of patients and study design, this study demonstrated that the perfusion–diffusion mismatch of MRI represents a depressed cerebral oxygen metabolism. The evolving infarct was associated with lower metabolic activity than the periinfarct. The metabolic penumbra with a relCMRO$_2$ ranging from 0.45 to 0.62 is a critical target for therapy by early reperfusion of occluded arteries, pharmacological neuroprotection, or both to reduce the volume expansion of brain infarction.

References

1. Warach S, Dashe JF, Edelman RR. Clinical outcome in ischemic stroke predicted by early diffusion-weighted and perfusion magnetic resonance imaging: a preliminary analysis. J Cereb Blood Flow Metab 1996;16:53–59.
2. Baird AE, Benfield A, Schlaug G, et al. Enlargement of human cerebral ischemic lesion volumes measured by diffusion-weighted magnetic resonance imaging. Ann Neurol 1997;41: 581–589.
3. Barber PA, Darby DG, Desmond PM, et al. Prediction of stroke outcome with echoplanar perfusion and diffusion-weighted MRI. Neurology 1998;51:418–426.
4. Beaulieu C, de Crespigny A, Tong DC, et al. Longitudinal magnetic resonance imaging study of perfusion and diffusion in stroke: evolution of lesion volume and correlation with clinical outcome. Ann Neurol 1999;46:568–578.
5. Karonen JO, Vanninen RL, Liu Y, et al. Combined diffusion and perfusion MRI with correlation to single-photon emission CT in acute ischemic stroke. Ischemic penumbra predicts infarct growth. Stroke 1999;30:1583–1590.
6. Neumann-Haefelin T, Wittsack HJ, Wenserski F, et al. Diffusion- and perfusion-weighted MRI. The DWI/PWI mismatch region in acute stroke. Stroke 1999;30:1591–1597.
7. Oppenheim C, Grandin C, Samson Y, et al. Is there an apparent diffusion coefficient threshold in predicting tissue viability in hyperacute stroke? Stroke 2001;32:2486–2491.
8. Rohl L, Ostergaard L, Simonsen CZ, et al. Viability thresholds of ischemic penumbra of hyperacute stroke defined by perfusion-weighted MRI and apparent diffusion coefficient. Stroke 2001;32:1140–1146.
9. Frackowiak RS, Lenzi GL, Jones T, et al. Quantitative measurement of regional cerebral blood flow and oxygen metabolism in man using ^{15}O and positron emission tomography: theory, procedure, and normal values. J Comput Assist Tomogr 1980;4: 727–736.
10. Herscovitch P, Markham J, Raichle ME. Brain blood flow measured with intravenous $H_2{}^{15}O$: theory, and error analysis. J Nucl Med 1983;24:782–789.
11. Mintun MA, Raichle ME, Martin WRW, et al. Brain oxygen utilization measured with O-15 radiotracers and positron emission tomography. J Nucl Med 1984;25:177–187.
12. Baron JC, Bousser MG, Rey A, et al. Reversal of focal "misery-perfusion syndrome" by extra-intracranial arterial bypass in hemodynamic cerebral ischemia. A case study with ^{15}O positron emission tomography. Stroke 1981;12:454–459.
13. Heiss WD, Grond M, Thiel A, et al. Tissue at risk of infarction rescued by early reperfusion: a positron emission tomography study in systemic recombinant tissue plasminogen activator thrombolysis of acute stroke. J Cereb Blood Flow Metab 1998; 18:1298–1307.
14. Derdeyn CP, Videen TO, Simmons NR, et al. Count-based PET method for predicting ischemic stroke in patients with symptomatic carotid arterial occlusion. Radiology 1999;212: 499–506.
15. Derdeyn CP, Videen TO, Grubb RL Jr, et al. Comparison of PET oxygen extraction fraction methods for the prediction of stroke risk. J Nucl Med 2001;42:1195–1197.
16. Schreiber WG, Gückel F, Stritzke P, et al. Cerebral blood flow and cerebrovascular reserve capacity: estimation by dynamic magnetic resonance imaging. J Cereb Blood Flow Metab 1998; 18:1143–1156.
17. Thijs VN, Adami A, Neumann-Haefelin T, et al. Relationship between severity of MR perfusion deficit and DWI lesion evolution. Neurology 2001;57:1205–1211.
18. Ibaraki M, Shimosegawa E, Miura S, et al. PET measurement of CBF, OEF, and CMRO$_2$ without arterial blood sampling in hyperacute ischemic stroke: methods and error analysis. Ann Nucl Med 2004;18:35–44.
19. Ardekani BA, Braun M, Hutton BF, et al. A fully automatic multimodality image registration algorithm. J Comput Assist Tomogr 1995;19:615–623.
20. Marchal G, Beaudouin V, Rioux P, et al. Prolonged persistence of substantial volumes of potentially viable brain tissue after stroke: a correlative PET-CT study with voxel-based data analysis. Stroke 1996;27:599–606.
21. Furlan M, Marchal G, Viader F, et al. Spontaneous neurological recovery after stroke and the fate of the ischemic penumbra. Ann Neurol 1996;40:216–226.
22. Giffard C, Young AR, Kerrouche N, et al. Outcome of acutely ischemic brain tissue in prolonged middle cerebral artery occlusion: a serial positron emission tomography investigation in the baboon. J Cereb Blood Flow Metab 2004;24:495–508.

23. Marchal G, Beaudouin V, Rioux P, et al. Prolonged persistence of substantial volumes of potentially viable brain tissue after stroke: a correlative PET-CT study with voxel-based data analysis. Stroke 1996;27:599–606.
24. Heiss WD, Huber M, Fink GR, et al. Progressive derangement of periinfarct viable tissue in ischemic stroke. J Cereb Blood Flow Metab 1992;12:193–203.
25. Back T, Hoehn-Berlage M, Kohno K, et al. Diffusion nuclear magnetic resonance imaging in experimental stroke. Correlation with cerebral metabolites. Stroke 1994;25:494–500.
26. Kohno K, Hoehn-Berlage M, Mies G, et al. Relationship between diffusion-weighted MR images, cerebral blood flow, and energy state in experimental brain infarction. Magn Reson Imaging 1995;13:73–80.
27. Qiao M, Malisza KL, Del Bigio MR, et al. Transient hypoxia-ischemia in rats: Changes in diffusion-sensitive MR imaging findings, extracellular space, and Na^+-K^+-adenosine triphosphatase and cytochrome oxidase activity. Radiology 2002;223: 65–75.
28. Hossmann K-A, Fischer M, Bockhorst K, et al. NMR imaging of the apparent diffusion coefficient (ADC) for the evaluation of metabolic suppression and recovery after prolonged cerebral ischemia. J Cereb Blood Flow Metab 1994;14:723–731.
29. Hoehn-Berlage M, Norris DG, Kohno K, et al. Evolution of regional changes in apparent diffusion coefficient during focal ischemia of rat brain: the relationship of quantitative diffusion NMR imaging to reduction in cerebral blood flow and metabolic disturbances. J Cereb Blood Flow Metab 1995;15: 1002–1011.
30. Sakoh M, Ostergaard L, Gjedde A, et al. Prediction of tissue survival after middle cerebral artery occlusion based on changes in the apparent diffusion of water. J Neurosurg 2001;95:450–458.
31. Rohl L, Ostergaard L, Simonsen CZ, et al. Viability thresholds of ischemic penumbra of hyperacute stroke defined by perfusion-weighted MRI and apparent diffusion coefficient. Stroke 2001;32:1140–1146.
32. Oppenheim C, Grandin C, Samson Y, et al. Is there an apparent diffusion coefficient threshold in predicting tissue viability in hyperacute stroke? Stroke 2001;32:2486–2491.
33. Baron JC, Bousser MG, Rey A, et al. Reversal of focal "misery-perfusion syndrome" by extra-intracranial arterial bypass in hemodynamic cerebral ischemia. A case study with ^{15}O positron emission tomography. Stroke 1981;12:454–459.
34. Young AR, Touzani O, Derlon JM, et al. Early reperfusion in the anesthetized baboon reduces brain damage following middle cerebral artery occlusion. A quantitative analysis of infarction volume. Stroke 1997;28:632–638.
35. Young AR, Sette G, Touzani O, et al. Relationships between high oxygen extraction fraction in the acute stage and final infarction in reversible middle cerebral artery occlusion: an investigation in anesthetized baboons with positron emission tomography. J Cereb Blood Flow Metab 1996;16:1176–1188.
36. Parsons MW, Barber A, Chalk J, et al. Diffusion- and perfusion-weighted MRI response to thrombolysis in stroke. Ann Neurol 2002;51:26–37.